

A central role for anterior cingulate cortex in the control of pathological aggression

Highlights

- Hyperaggressive mice show widespread cell death in anterior cingulate cortex (ACC)
- Hyperaggressive mice fail to activate ACC during confrontations
- Boosting ACC activity eliminates pathological, but not species-typical, aggression
- This is linked to rebalanced activity in downstream areas, e.g., amygdala

Authors

Sabrina van Heukelum, Kerli Tulva, Femke E. Geers, ..., Brent A. Vogt, Martha N. Havenith, Arthur S.C. França

Correspondence

sabrina.vanheukelum@radboudumc.nl

In brief

Aggression is a core aspect of behavior. How does it turn pathological? van Heukelum et al. highlight anterior cingulate cortex (ACC) as a potential switch: in hyperaggressive mice, ACC is structurally degraded and hypoactive during confrontations. Boosting ACC activity eliminates pathological aggression but preserves species-typical aggression.



Article

A central role for anterior cingulate cortex in the control of pathological aggression

Sabrina van Heukelum,^{1,2,11,*} Kerli Tulva,^{1,2} Femke E. Geers,^{1,2} Sanne van Dulm,^{1,2} I. Hyun Ruisch,^{1,3} Jonathan Mill,⁴ Joana F. Viana,⁵ Christian F. Beckmann,^{1,2} Jan K. Buitelaar,^{1,2} Geert Poelmans,^{1,3} Jeffrey C. Glennon,^{1,2,6,10} Brent A. Vogt,^{7,8,10} Martha N. Havenith,^{1,2,9,10} and Arthur S.C. França^{1,2,10}

¹Donders Institute for Brain, Cognition and Behaviour, Radboudumc, Nijmegen, the Netherlands

²Department of Cognitive Neuroscience, Radboudumc, Nijmegen, the Netherlands

³Department of Human Genetics, Radboud University Medical Centre, Nijmegen, the Netherlands

⁴University of Exeter Medical School, University of Exeter, Exeter, UK

⁵The Institute of Metabolism and Systems Research (IMSR), University of Birmingham, Edgbaston, Birmingham, UK

⁶Conway Institute of Biomolecular and Biomedical Research, School of Medicine, University College Dublin, Belfield, Dublin, Ireland

⁷Cingulum Neurosciences Institute, Manlius, NY, USA

⁸Department of Anatomy and Neurobiology, Boston University School of Medicine, Boston, MA, USA

⁹Zero-Noise Lab, Ernst Strüngmann Institute for Neuroscience, 60528 Frankfurt a.M., Germany

¹⁰These authors contributed equally

¹¹Lead contact

*Correspondence: sabrina.vanheukelum@radboudumc.nl

<https://doi.org/10.1016/j.cub.2021.03.062>

SUMMARY

Controlling aggression is a crucial skill in social species like rodents and humans and has been associated with anterior cingulate cortex (ACC). Here, we directly link the failed regulation of aggression in BALB/cJ mice to ACC hypofunction. We first show that ACC in BALB/cJ mice is structurally degraded: neuron density is decreased, with pervasive neuron death and reactive astroglia. Gene-set enrichment analysis suggested that this process is driven by neuronal degeneration, which then triggers toxic astrogliosis. cFos expression across ACC indicated functional consequences: during aggressive encounters, ACC was engaged in control mice, but not BALB/cJ mice. Chemogenetically activating ACC during aggressive encounters drastically suppressed pathological aggression but left species-typical aggression intact. The network effects of our chemogenetic perturbation suggest that this behavioral rescue is mediated by suppression of amygdala and hypothalamus and activation of mediodorsal thalamus. Together, these findings highlight the central role of ACC in curbing pathological aggression.

INTRODUCTION

Aggression is an evolutionarily conserved behavior present in most species, including humans. What is more, when applied in a context-appropriate way, e.g., by defending against intruders, aggression is a crucial survival skill.^{1–5} In contrast, dysfunctional aggression, such as abusive and anti-social behavior, leads to severe long-term personal and societal harm^{1,6} and is often observed in the context of different psychiatric disorders, including borderline personality disorder, psychopathy, and conduct disorder.⁷ What could be the neuronal mechanisms underlying such pathological aggression?

Aggressive behavior can generally be thought of as the product of two interconnected and complementary—even at times antagonistic—cortical and subcortical networks. One network, also referred to as the threat circuit,⁸ centers on the bed nucleus of the stria terminalis as well as the (ventromedial) hypothalamus and amygdala, which integrate information on potential threats, and initiates aggressive output via the periaqueductal gray (PAG).^{8,9} In line with this, studies in rodents show that stimulating the hypothalamus^{10–12} and specific neural populations within the

amygdala^{13,14} can trigger aggressive behavior. A second network, including cingulate cortex, prefrontal cortex, lateral septum, and insula, is thought to mediate the top-down regulation of aggression in humans,^{6,8} rodents,^{15–20} and other mammals^{21–24} by modulating subcortical circuits.²⁵

Within this network, cingulate cortex, and specifically anterior cingulate cortex (ACC), seems to have a crucial gating function for aggressive behavior. For instance, in wild-type rodents, inhibiting ACC leads to increased aggression in response to territorial challenge, although boosting ACC in the same animals reduces aggressive behavior.¹⁷ Given ACC's capacity to titrate aggressive behavior, it seems plausible that it would play a central role both in the development and in the treatment of pathological aggression.⁶ So far, this notion has been supported by several correlative observations in both humans and rodents. For instance, studies in patients with pathological aggression demonstrate alterations in ACC volume^{26,27} as well as ACC activity.^{27,28} Consistently with this, the BALB/cJ strain, a mouse model of pathological aggression, shows a volumetric increase of ACC compared to the non-aggressive BALB/cByJ control strain,²⁹ as well as a decrease of parvalbumin- and



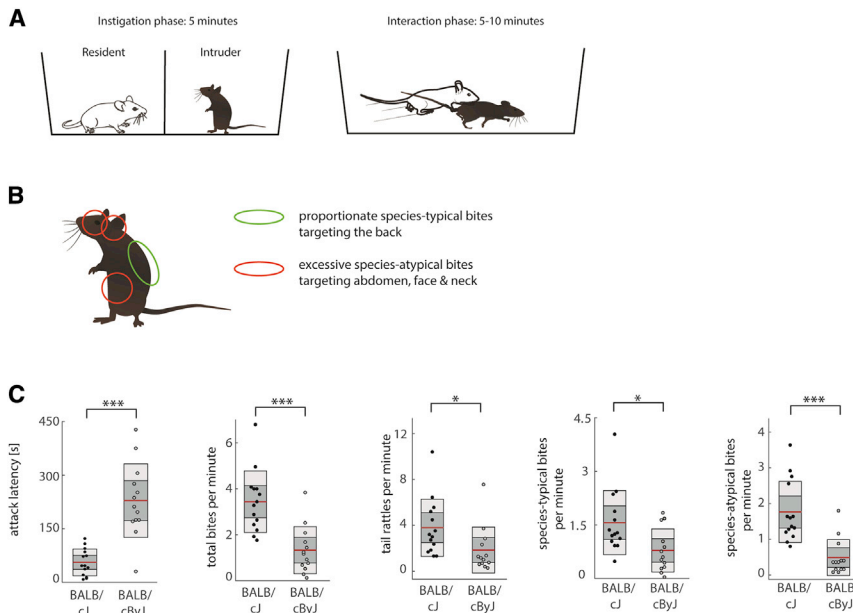


Figure 1. Aggression paradigm and behavioral metrics

(A) Schematic of the RI test, depicting the instigation phase (left) and the interaction phase (right). (B) Schematic showing possible bite spots, divided into species-typical and species-atypical bites (see in-figure legend). (C) Average attack latency, total bites, tail rattles, species-typical bites, and species-atypical bites. Black dots, BALB/cJ mice; gray dots, BALB/cByJ mice. Shown are average (red line), 95% confidence interval (dark gray area), and 1 SD (light gray area). * $p < 0.05$; ** $p < 0.01$; *** $p < 0.001$. See also [Figure S1](#) and [Video S1](#).

somatostatin-expressing interneurons across cingulate cortex.³⁰ In addition, in isolation-reared rats exhibiting increased aggressive behavior, ACC was less activated by aggressive encounters.³¹

Although these structural and functional observations indicate that abnormalities in ACC are closely linked to the occurrence of pathological aggression, the processes establishing this link are unclear. First, the structural alterations driving ACC impairment in pathological aggression have remained largely unaddressed. Here, we characterized structural and functional characteristics of ACC in the BALB/cJ strain. On a structural level, we discovered pervasive neuron death, accompanied by toxic glial processes, which resulted in stark reductions of neuronal density compared to control mice. These degenerative processes were focused on ACC, with neighboring areas, such as secondary motor cortex (M2) and somatosensory cortex (S1), remaining largely unaffected. On a functional level, cFos expression indicated that BALB/cJ mice failed to activate ACC during aggressive encounters. These findings highlight structural degeneration in ACC as a hallmark of pathological aggression.

Most importantly, even though there is strong structural and functional indication that ACC degeneration is one of the drivers of pathological aggression, it is not clear whether re-instating ACC activity is sufficient to rescue species-typical aggressive behavior. After all, ACC malfunction may have initially unbalanced the circuits regulating context-appropriate aggression, but simply recovering ACC activity may not promptly rebalance these circuits. Here, we provide evidence that ACC activation directly rescues context-appropriate aggression in BALB/cJ mice. Specifically, we found that chemogenetically activating ACC in BALB/cJ mice was sufficient to prevent pathological aggression, although having a negligible effect on species-typical aggressive behaviors. Analysis of cFos expression following our chemogenetic intervention revealed that this behavioral rescue was most likely mediated not only by increased activity in ACC itself but also by downstream effects

eliminate excessively aggressive acts in a mouse model of pathological aggression.

RESULTS

Structural degradation in ACC of aggressive BALB/cJ mice

To quantify species-typical and excessive aggression in BALB/cJ mice and control BALB/cByJ mice, we applied the resident-intruder (RI) test. In the RI test, an unfamiliar “intruder” mouse is introduced into the home cage of the test mouse (also referred to as the resident). After an initial “instigation phase” of 5 min, a barrier between the animals is lifted, and animals interact for 5–10 min before the intruder is removed ([Figure 1A](#); see [STAR Methods](#) and [Figure S1](#) for details). A new encounter then takes place daily for 5 days in a row ([Figure 1A](#)). Behavior during the interaction phase is scored for threats (tail rattles), as well as different types of attack, specifically to the back, neck, face, and abdomen, and the latency of the first attack (see [Video S1](#) for examples).

Based on these metrics, we classified aggressive behaviors either as species-typical or as pathological. A clear-cut definition of pathological aggression can of course be difficult to determine. For instance, what level of aggression is maladaptive for a predator versus a prey animal? Here, we define pathological aggression as any aggressive act that causes harm to the opponent beyond the species-typical level. In the case of territorial disputes in mice, species-typical behavior would generally consist of threats in the form of tail rattles as well as some bites to robust body parts, like the back. In contrast, bites to vulnerable body parts, like the neck, face, and belly (as well as prolonged bites to robust body parts), would be considered species-atypical ([Figure 1B](#)).^{29,30,32,33}

In line with previous reports,^{29,30,34} BALB/cJ mice consistently behaved more aggressively than control BALB/cByJ mice: they attacked faster ($F(1, 25) = 34.65$; $p < 0.001$; $\eta^2 = 0.58$; [Figure 1C](#))

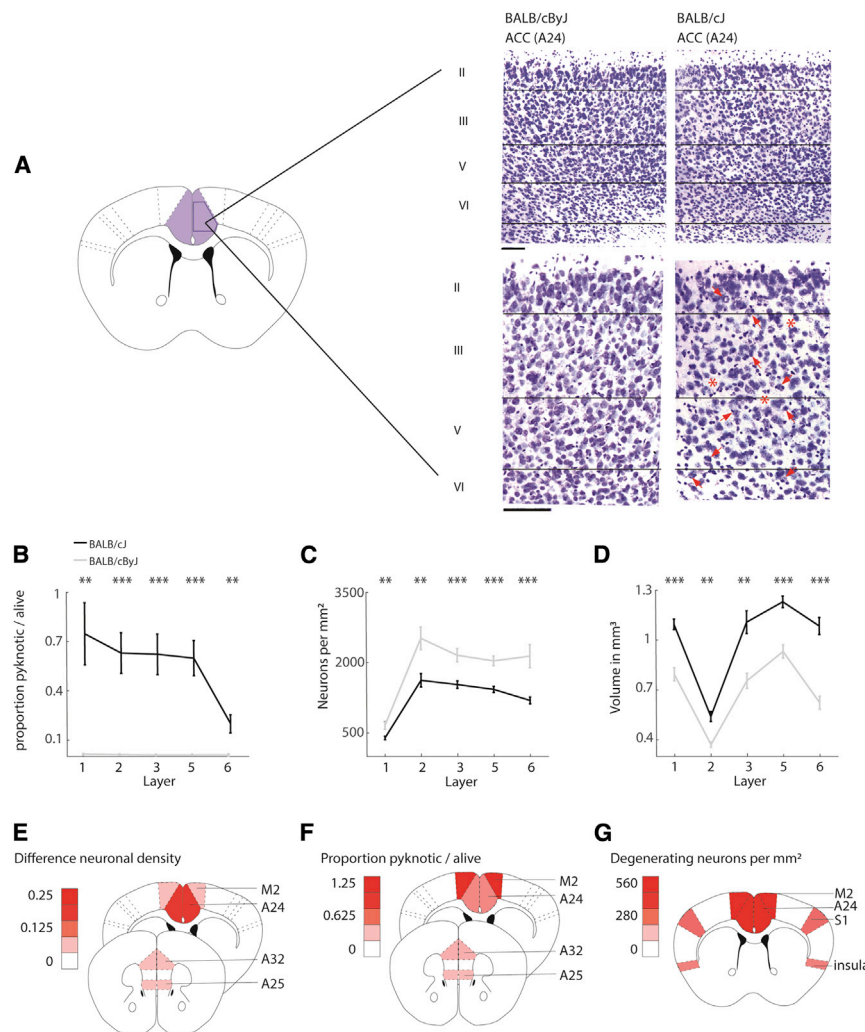


Figure 2. Cytoarchitecture of ACC

(A) Schematic of area 24 of ACC. Inset: photographs in different magnifications show the outlines of the position of layers. Pyknotic neurons are noted with red arrows in the high-magnification BALB/cJ case. There are also 3 red asterisks to emphasize places where there are clearings with no neurons to emphasize their loss. Scale bars, 100 μm .

(B) The proportion of pyknotic/non-pyknotic neurons. Black line, BALB/cJ mice; gray line, BALB/cByJ mice. Shown are average and SEM per layer.

(C) The number of neurons per mm^2 . Shown are average and SEM per layer.

(D) The total volume in mm^3 . Black line, BALB/cJ mice; gray line, BALB/cByJ mice. Shown are average and SEM per layer. * $p < 0.05$; ** $p < 0.01$; *** $p < 0.001$.

(E) Heatmap of the difference in neuronal density between BALB/cJ and BALB/cByJ mice for A24, A25, A32, and M2.

(F) Heatmap for the proportion pyknotic/alive neurons, same regions as in (E).

(G) Heatmap for the number of degenerating neurons per mm^2 across A24, M2, S1, and insula. See also [Figures S2](#) and [S3](#).

and more frequently ($F(1, 25) = 20.93$; $p < 0.001$; $\eta^2 = 0.46$; [Figure 1C](#)). What is more, when differentiating between species-typical and pathological forms of aggression, species-typical aggression in the form of tail rattles ($F(1, 25) = 4.6$; $p = 0.048$; $\eta^2 = 0.17$) and back bites ($F(1, 25) = 6.9$; $p = 0.03$; $\eta^2 = 0.22$) was significantly elevated in BALB/cJ mice, yet the starkest increase occurred in species-atypical attacks targeting vulnerable body parts ($F(1, 25) = 21.8$; $p = 0.001$; $\eta^2 = 0.47$). [Figure S1A](#) tracks aggressive behavior across individual days of the RI test, and [Figure S1B](#) demonstrates persistent differences in aggression across two different variants of the RI test where interaction time was limited to 5 min, starting either with the removal of the barrier or with the first attack ([STAR Methods](#)).

Based on the hypothesis that excessive aggression might arise from impaired top-down regulation by ACC,^{6,17,18} we first examined structural changes in ACC, specifically in Brodmann area 24 (A24). We performed a Cresyl violet staining that enabled us to assess structural features of neurons ([Figure 2A](#)). Across all layers of A24, we found high rates of pyknotic neurons ([Figure 2B](#); repeated-measure ANOVA, with strain as between-subject factor and layer as within-subject factor: $F(1, 31) = 18.69$,

$p < 0.001$, $\eta^2 = 0.38$; post hoc t tests per layer: all $p < 0.01$). During pyknosis, the chromatin in the nucleus of a cell condenses, an irreversible process that occurs during cell death.³⁵ As such, our data show that a large number of ACC neurons are dying in BALB/cJ mice. In line with this, unbiased stereological counting using Stereoinvestigator (MBF Biosciences) revealed that neuron densities in A24 were drastically decreased across all cortical layers ([Figure 2C](#); repeated-measures ANOVA: $F(1, 31) = 23.05$, $p < 0.001$, $\eta^2 = 0.43$; post hoc t tests per layer: all $p < 0.01$). In BALB/cByJ mice, A24 contained on average 55% more neurons (1,886 neurons/ mm^2) than in BALB/cJ mice (1,219 neurons/ mm^2 ; [Figure 2C](#)). To exclude the possibility that the RI test itself might affect ACC structure, we also included BALB/cJ animals ($n = 6$) in our analyses that had not experienced the RI test. Neither measures of neuron death nor neuron density showed differences depending on whether animals were subjected to the RI test, suggesting that the observed effects are not induced by our behavioral testing ([Figures S2A](#) and [S2B](#)).

To probe whether the measured neuron death in ACC is likely to reflect a local or a brain-wide process in BALB/cJ mice, we also quantified pyknosis and neuron density in neighboring sub-areas of ACC, specifically Brodmann areas 25 and 32 (A25 and A32), as well as in M2, which directly borders on ACC. The loss of neuron density was negligible for all three neighboring areas, particularly M2, suggesting that decreased neuron density is a largely localized phenomenon ([Figure 2G](#); see also [Figure S3](#)). In contrast, all three neighboring areas featured high proportions of pyknotic neurons similar to those in A24 ([Figure 1E](#);

see also Figure S3). Based on these results, we wanted to further verify how widespread the observed neuronal degeneration was across the brain. To this end, we performed a second staining specifically targeted toward degenerating neurons (Fluoro-Jade C)³⁶ and included two additional areas more distant from A24—S1 (about 2.5 mm lateral distance to ACC) and insula (about 4.5 mm lateral distance to ACC). Again, we observed high levels of degenerating neurons in both A24 and M2 of BALB/cJ mice but few in S1 and even fewer in insula (Figure 1F; see also Figure S3).

This dissociation between widespread neuronal degeneration and localized loss of neuron density appears to be most compatible with a scenario in which neuronal degeneration is spreading, but the absorption of dead cells is impaired. Such ineffective clearance of dying cells has been implicated in inflammatory and neurodegenerative conditions.^{37,38} This process would seem to have advanced furthest in A24, with neuronal degeneration already resulting in decreased neuron density. In neighboring A25, A32, and M2, increased neuronal degeneration has not yet impacted neuronal density due to slow clearance of dying cells, and distant areas, such as S1, only show small amounts of neuronal degeneration.

Interestingly, despite the dramatic amount of neuronal death and decreased neuronal density across all layers of ACC, BALB/cJ mice showed an increased volume of ACC compared to BALB/cByJ mice (Figure 2D; repeated-measures ANOVA: $F(1, 8) = 45.46$, $p < 0.001$, $\eta^2 = 0.85$; $n = 5$ per group; see also van Heukelum et al.²⁹). This suggests that dead neurons must have been replaced by other cells that extend or “bloat” ACC, with the most likely candidate being glial cells.

Increased neurotoxicity of astroglia aligns with neuronal death

Because both microglia and astroglia are activated by neuronal insult, we tested whether the widespread cell death and volume increase in ACC coincided with abnormal glial processes and whether glial populations were generally increased ($n = 15$ BALB/cJ and 14 BALB/cByJ mice—cohort 1 to 2 and 6 mice per strain not subjected to the RI test). We stained for microglia and astroglia and then differentiated between dormant and reactive astroglia by determining the percentage of reactive toxic (A1) astroglia.

In ACC, we found a clear increase in the number of microglia (marker: Iba1) in BALB/cJ mice compared to control mice (Figures 3A and 3B; repeated-measures ANOVA: $F(1, 27) = 7.79$; $p = 0.02$; $\eta^2 = 0.22$). Post hoc tests revealed that these differences were layer specific (Figure 2B): increases in microglia were restricted to layers 1 (post hoc t tests; $p < 0.001$) and 5 ($p < 0.05$). We next stained for the total number of astroglia (marker S100B), irrespective of their activity state, and observed increases in the number of astroglia in ACC ($F(1, 27) = 9.73$; $p = 0.008$; $\eta^2 = 0.26$), which were again layer specific (post hoc t tests; layers 1 and 6; Figures 3C and 3D). In a next step, we identified reactive astrogliosis by a GFAP staining^{39,40} and observed dramatic increases in the number of GFAP-positive astroglia across all layers in BALB/cJ mice (Figures 3E and 3F; repeated-measures ANOVA: ACC: $F(1, 27) = 136.83$; $p < 0.001$; $\eta^2 = 0.84$). In some layers, an up to 10-fold increase occurred, suggesting reactive astrogliosis may

be responsible for the increased volume of ACC observed here and previously.²⁹

To decipher whether the observed reactive astroglia were toxic A1 astroglia, we performed a co-staining of Serping1 (marker upregulated in A1 astroglia) with S100B (general marker for astroglia). Our data show an upregulation of Serping1 in astroglia, suggesting neurotoxic A1 astroglia in BALB/cJ mice compared to BALB/cByJ mice across all layers of ACC (Figures 3G and 3H; repeated-measures ANOVA: $F(1, 27) = 13.9$, $p = 0.003$, $\eta^2 = 0.34$; post hoc t tests: all $p < 0.001$; Figure 2D). This is in line with the high levels of pyknosis we detected, as A1 astroglia are known to induce cell death.⁴¹ As for other metrics, there were again no differences between mice that participated in the RI test and those that did not (Figure S2). Interestingly, we also did not observe significant differences in overall microglia or astroglia populations in A25, A32, or M2, and although we saw an increased number of reactive astroglia in these three regions, we did not see an upregulation of toxic A1 astroglia (Figure S3). This is again consistent with the interpretation that structural degradation is most advanced in A24, which features a combination of pyknotic neurons, reduced neuron density, and high amounts of toxic astroglia. In contrast, A25, A32, and M2 show increased numbers of pyknotic neurons but no change in neuron density or toxic astroglia, suggesting earlier stages of degeneration.

Gene-set enrichment analysis reveals genetic drivers of neuron death

To further investigate which molecular pathways were implicated in the observed neuron death throughout ACC, we applied gene-set enrichment analysis of genetic differences between BALB/cJ and BALB/cByJ strains, obtained from whole-genome sequencing data. Single-nucleotide variants (SNVs) that differed between the two strains were annotated to a total of 1,541 genes that were subsequently subdivided into 3 different categories: intronic/exonic non-coding and synonymous variants (1,422 genes), untranslated region (UTR) variants (3' and 5'; 90 genes), and missense mutations and splicing variants (61 genes). To analyze these genetic differences, we utilized the ingenuity pathway analysis software package (IPA) (QIAGEN). Four different analyses were performed: (1) IPA on genes annotated to the whole set of SNVs; (2) IPA on genes annotated to intronic/exonic non-coding/synonymous variants; (3) IPA on genes annotated to UTR variants; and (4) IPA on genes annotated to missense mutations and splicing variants. Data analysis was hypothesis driven, and we report the results for the “cell death and survival” category and its subcategories as provided by IPA (only categories that show at least 2 affected molecules).

All genes annotated to SNV differences in BALB/c strains (1,514 genes)

IPA analysis of all SNVs were in line with our histological data: we found clear indications for genetic differences between BALB/cJ and BALB/cByJ mice related to cell death. Not only did IPA reveal differences in SNVs associated with apoptosis and necrosis, but it specifically pointed toward degeneration of neurons and loss of brain cells (Table S1). As such, this is not only in line with the observed neuronal death but also the reduced neuronal density in ACC of aggressive BALB/cJ mice.

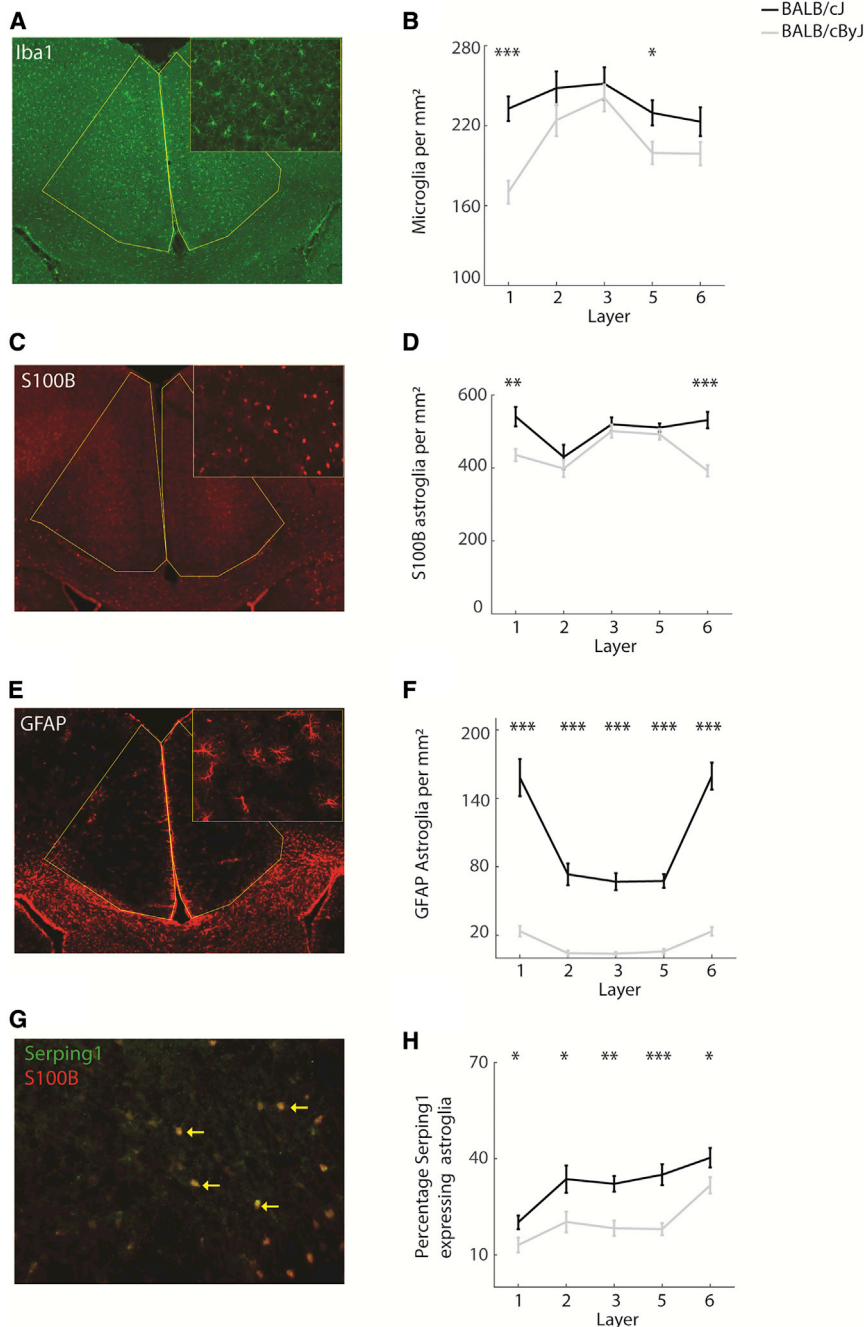


Figure 3. Microglia and astroglia across ACC layers

(A) Example photograph of microglia across layers. (B) The number of microglia per mm² across layers. Black line, BALB/cJ mice; gray line, BALB/cByJ mice. Shown are average and SEM. (C and D) Same as (A) and (B) for S100B-positive stained astroglia across layers. (E and F) Same as (A) and (B) for GFAP-positive stained astroglia. (G) Example photograph of S100B astroglia double stained with a marker for toxic astroglia (Serping1, yellow arrow). (H) The percentage of toxic astroglia. Shown are average and SEM. *p < 0.05; **p < 0.01; ***p < 0.001. See also Figures S2 and S3.

within cell death and survival specifically pointed to neuron degeneration and the loss of brain cells (Table S1).

Genes annotated to UTR SNV differences in BALB/c strains (90 genes)

IPA analysis of the UTR variants revealed SNV differences between the strains to be enriched for apoptosis of pericytes, erythroid precursor cells, and erythroblasts. Even though degeneration of neurons was not highlighted in this analysis, the affected SNVs are also annotated to genes that overlap with genes from the whole dataset found to be involved in the degeneration of neurons.

Genes annotated to missense mutations and splicing region SNV differences in BALB/c strains (61 genes)

Similar to the UTR analysis, the missense mutations and splicing variants did not show enrichment for neuron degeneration. The only significantly enriched category here was cytolysis of lymphocytes. Nevertheless, as with the UTR variants, the affected SNVs were also annotated to genes that were part of the category “degeneration of neurons.” The relatively low number of genes annotated to

Interestingly, we did not observe significant enrichment of categories related to glial involvement (after expanding the analysis to the nervous system category that contains the glial-related genes), suggesting that neuronal death is not a consequence of rogue glia but rather that glial processes are only activated upon neuronal death.

Genes annotated to intronic/exonic non-coding and synonymous SNV differences in BALB/c strains (1,422 genes)

We subsequently looked at the intronic/exonic non-coding and synonymous variants separately, and again, the categories

missense/splicing variants as well as UTR SNVs may, however, prohibit enrichment of the neuron degeneration category.

Functional consequences of structural degradation

Given the stark structural changes detected in ACC, we hypothesized that ACC function would also be impacted and therefore stained for the activity marker cFos (Figure 4A). At baseline, when animals had never been subjected to the RI test, there were no significant differences in ACC activity between BALB/cJ and BALB/cByJ mice (Figure 4B; $F(1, 10) = 1.26$; $p = 0.39$; $\eta^2 = 0.11$; $n = 6$ per strain). To track activity levels during

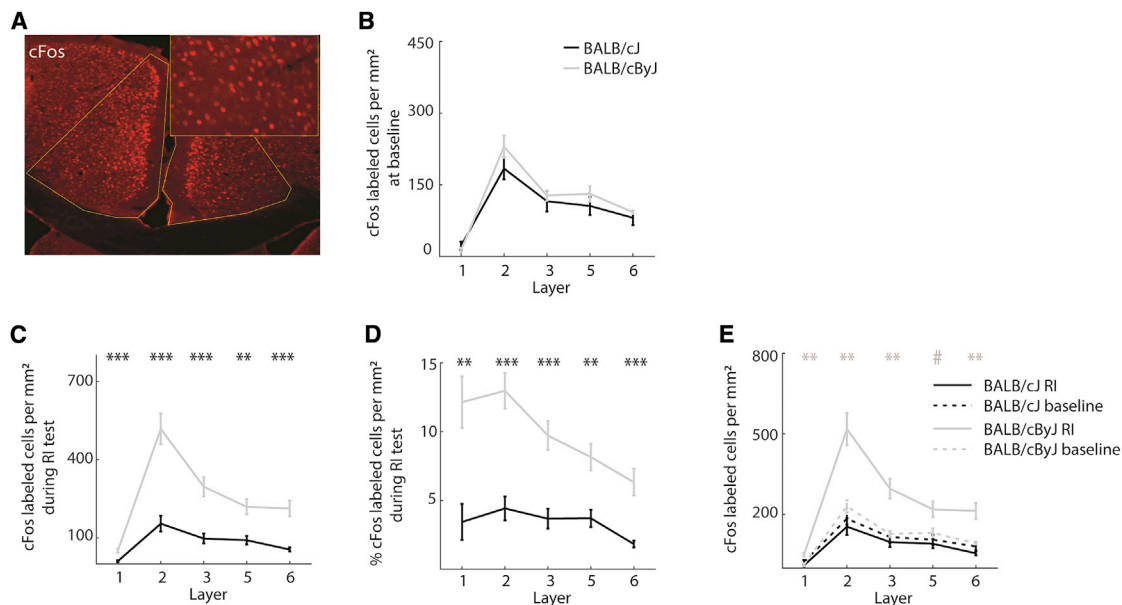


Figure 4. Activity levels

(A) Example photograph of stained cFos cells.

(B) The number of cFos-labeled cells in per mm² at baseline. Black line, BALB/cJ mice; gray line, BALB/cByJ mice.

(C) The number of cFos-labeled cells per mm² during the last day of the RI test.

(D) Same as (B) but expressed as percentage of total neuron density.

(E) Comparison of activity at baseline versus RI for BALB/cJ and BALB/cByJ mice. See in-figure legend; gray asterisks refer to statistical comparisons within the BALB/cByJ group only.

(B)–(E) show the average and SEM per layer.

p* < 0.05; *p* < 0.01; ****p* < 0.001. See also [Figures S2–S4](#).

aggressive encounters, we sacrificed animals 45–60 min after the last RI to allow for optimal cFos expression levels (*n* = 9 BALB/cJ and 8 BALB/cByJ).⁴² Interestingly, after aggressive encounters, cFos markers revealed a lack of engagement of ACC in BALB/cJ mice: on average, BALB/cJ mice activated 82 neurons/mm²—less than a third of the 259 neurons/mm² activated by BALB/cByJ mice across all layers of ACC ([Figure 4C](#), left panel; $F(1, 15) = 32.6$; $p < 0.001$; $\eta^2 = 0.69$). This difference also held when we controlled for general neuron density across all layers of ACC ([Figure 4D](#); $F(1, 15) = 28.34$; $p < 0.001$; $\eta^2 = 0.66$). As a consequence, ACC activity was clearly elevated after the RI test compared to baseline in BALB/cByJ mice ([Figure 4E](#); $F(1, 11) = 16.78$; $p < 0.001$; $\eta^2 = 0.58$), but not in BALB/cJ mice ([Figure 4E](#); $F(1, 13) = 0.95$; $p = 0.351$; $\eta^2 = 0.07$). This suggests that, although the structural degradation of ACC in BALB/cJ mice does not significantly impact resting ACC activity, it results in a failure to activate ACC during aggressive encounters.

Restoring ACC activity prevents escalatory aggression

Based on the observed hypofunction of ACC in BALB/cJ mice, we examined whether increasing ACC activity would be sufficient to prevent the escalation of pathological aggressive behavior. We chose to boost ACC activity chemogenetically: in one group of BALB/cJ mice, an excitatory designer receptor exclusively activated by designer drug (DREADD) (CaMKIIa promoter; hM3D(Gq receptor)) was injected bilaterally into A24, while the other group only received a sham virus containing a fluorescent protein. RI tests were performed 2 weeks after

surgeries, and all mice received clozapine-N-oxide (CNO) injections 30 min before testing to ensure that there are no off-target effects of the CNO.

Histology confirmed that virus expression in both groups was strong in A24, with minimal bleeding into neighboring M2 ([Figures 5A and 5B](#)). Since our previous experiments demonstrated that M2 is not specifically recruited during aggressive encounters, this minimal expression within M2 is unlikely to have had relevant behavioral effects. cFos histology confirmed that we indeed increased ACC activity in the hM3D group compared to the sham virus group by an average rate of 40% ([Figure 5C](#); $F(1, 10) = 12.34$, $p = 0.01$, $\eta^2 = 0.53$; *n* = 7 hM3D group and 5 sham virus group). On the behavioral level, we observed a marked decrease of aggression in the hM3D group compared to the sham virus group ([Figure 5D](#)): mice attacked later ($F(1, 10) = 11.77$; $p = 0.008$; $\eta^2 = 0.54$) and carried out fewer total bites ($F(1, 10) = 39.8$; $p < 0.001$; $\eta^2 = 0.8$; [Figure 5D](#)). What is more, correlation analysis suggested a direct linear relationship between cFos markers of ACC activity during the RI test and physical aggression: the higher ACC activity, the less physical aggression occurred ([Figure 5D](#); all $R^2 > 0.45$; all $p < 0.02$ after correction for multiple comparisons). Behavioral differences across individual sessions of the RI test can be found in [Figure S3](#).

Interestingly, when differentiating species-typical and species-atypical attacks in the hM3D group, the reduction in species-atypical bites was most pronounced ($F(1, 10) = 36.3$; $p < 0.001$; $\eta^2 = 0.78$). Species-typical back bites decreased less dramatically ($F(1, 10) = 20.6$; $p = 0.002$; $\eta^2 = 0.67$), and there

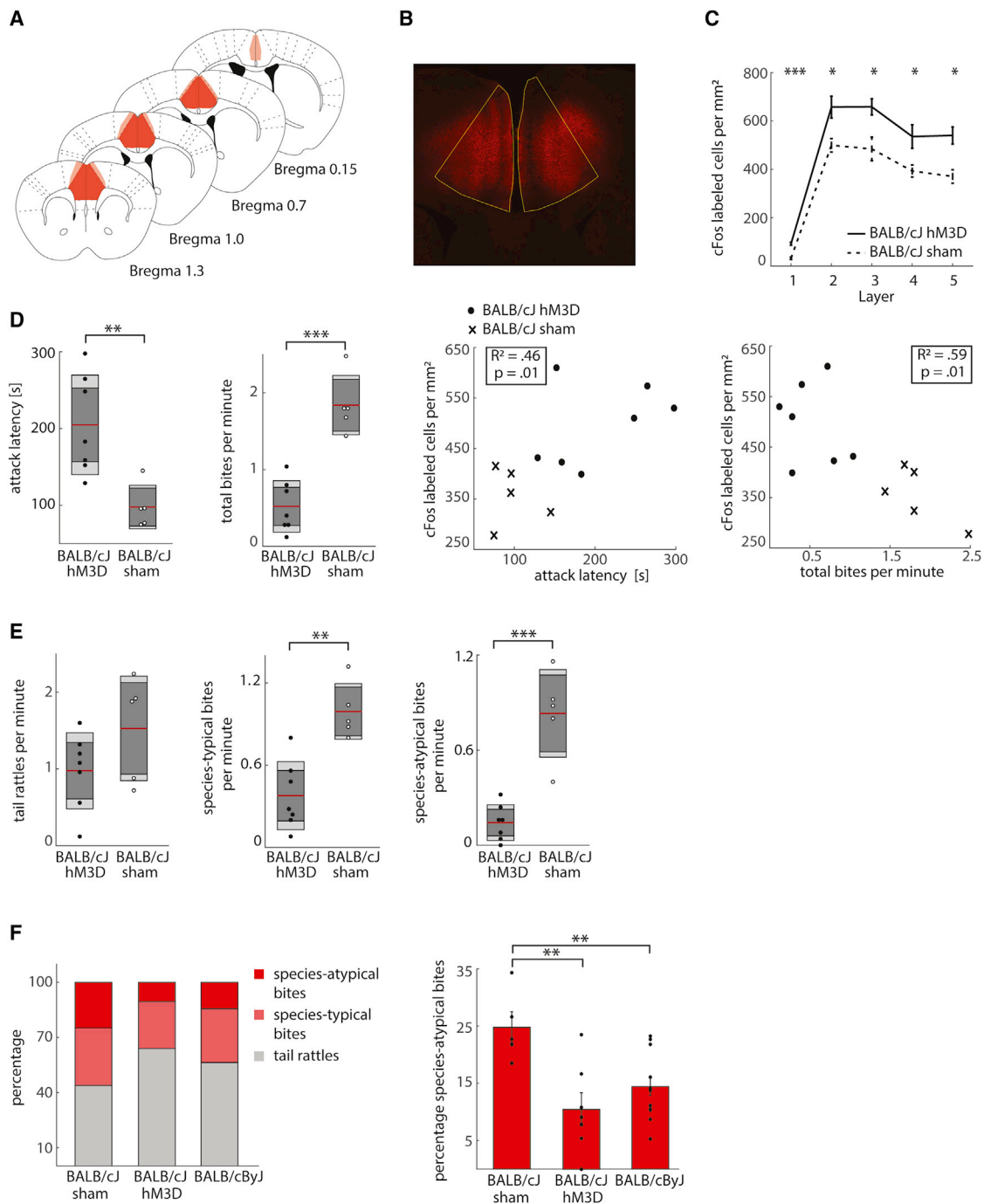


Figure 5. Chemogenetic manipulation of ACC activity

(A) Verification of virus expression; bright red, strong expression; light red, sparse expression.

(B) Example image of mCherry expression outlining the spread of the viral DREADD vector; yellow outline, ACC.

(C) Average of cFos-labeled cells across ACC layers. Solid line, hM3D DREADD group; dashed, Sham virus BALB/cJ mice. Error bars: SEM.

(D) Boxplots: average attack latency and average total bites. Black dots, BALB/cJ mice injected with hM3D virus; white dots, BALB/cJ mice injected with sham virus; red line, average; dark gray area, 95% confidence interval; light gray area, 1 SD; scatterplots, correlations between average ACC activity and attack latency (left) and total bites (right); dots, BALB/cJ mice injected with hM3D virus; crosses, Sham BALB/cJ mice.

(E) Same as boxplots in (B) for tail rattles, species-typical bites, and species-atypical bites.

(F) Left: percentage of aggressive acts, subdivided into tail rattles and species-typical and species-atypical bites for BALB/cJ sham mice, BALB/cJ mice injected with hM3D virus and control BALB/cByJ mice. Right: same as left for percentage of species-atypical bites; shown are also individual data points.

* $p < 0.05$; ** $p < 0.01$; *** $p < 0.001$. See also [Figure S5](#).

was no difference in non-violent threat behavior, i.e., tail rattles (Figure 5E; $F(1, 10) = 2.7$; $p = 0.13$; $\eta^2 = 0.21$). These reductions suggest that animals in the hM3D group reverted to a species-typical response pattern to territorial challenge. To directly quantify whether responses in the hM3D group were indeed indistinguishable from those of BALB/cByJ mice, we compared the relative proportion of different attack types for treated and untreated BALB/cJ mice to that of BALB/cByJ mice (Figure 5F). The overall balance between non-physical, species-typical, and pathological acts of aggression in the hM3D group was statistically indistinguishable from that of BALB/cByJ mice but differed significantly from that of untreated BALB/cJ mice (repeated-measures ANOVA hM3D versus BALB/cByJ: $F(1, 18) = 1.15$, $p = 0.3$, $\eta^2 = 0.06$; hM3D versus sham, interaction effect: $F(2, 20) = 6.1$, $p = 0.009$, $\eta^2 = 0.38$). Specifically, the portion of species-atypical attacks decreased to 10.5% in the hM3D group—a percentage that is significantly lower ($F(1, 10) = 8.3$; $p = 0.02$; $\eta^2 = 0.45$) than the 24.8% observed in the sham virus group, but not significantly different from the 14.4% observed in BALB/cByJ animals (Figure 5F). In contrast, the proportion of species-typical back bites remained comparable, fluctuating around 30% across all three groups (hM3D versus sham: $F(1, 10) = 1.2$, $p = 0.3$, $\eta^2 = 0.11$; sham versus BALB/cByJ: $F(1, 16) = 1.3$, $p = 0.27$, $\eta^2 = 0.08$), although the proportion of tail rattles was significantly increased from 44% to 64% in the hM3D versus the sham BALB/cJ group ($F(1, 10) = 6.68$; $p = 0.03$; $\eta^2 = 0.4$). Together, both the absolute frequency of physical attacks and the relative proportion of different aggressive acts suggest that increased ACC activity specifically curbed species-atypical aggression but left species-typical aggression, and particularly non-physical aggression, intact (Figures 5E and 5F).

To understand how ACC activity is able to curb pathological aggression, we probed its effect on downstream structures by applying cFos staining to prominent efferent regions, specifically the basolateral amygdala (BLA), the lateral hypothalamus (LH), the ventromedial hypothalamus (VMH), and the mediodorsal thalamus (MD). BLA, LH, and VMH are considered part of the threat circuit,^{43,44} whereas MD has been associated with flexible goal-directed behavior.^{45,46} We saw direct efferent projections from ACC to BLA, LH, and MD but none to VMH (Figure 6A). However, because LH is known to project to VMH,⁴⁷ we decided to include VMH in our analyses as a disynaptic target region. For BLA, LH, and VMH, we observed substantial decreases in activity in the hM3D group compared to the sham virus group, although activity in MD increased (all $p < 0.05$; Figure 6B; see Figure S5 for activity per sub-area of these structures). When relating activity within these regions to behavioral metrics, we observed that activity within BLA, LH, and VMH all correlated positively with the overall amount of aggressive attacks (Figures 6D–6G; all $R^2 > 0.35$; all $p < 0.05$ after correction for multiple comparisons), although MD activity correlated negatively with aggressive behavior: higher MD activity was associated with fewer bites ($R^2 = 0.56$; $p = 0.02$). In line with previous work,^{12,18,19} these results suggest that all these downstream regions are jointly involved in computations regarding the intensity of aggressive acts. In contrast, out of the regions tested here, only BLA also reflected the initial drive to attack: its activity was negatively correlated with attack

latency ($R^2 = 0.50$, $p = 0.04$; all other $R^2 < 0.35$, all other $p > 0.1$; Figure S6).

To control whether our chemogenetic manipulation may have resulted in a non-specific activation of cortical activity beyond the known efferent regions of ACC, we also checked cFos expression in M2 and S1 of the DREADD group. We did not observe any differences in activity here, neither for M2 (Figure 6C; ANOVA: $F(1, 10) = 3.07$; $p = 0.13$; $\eta^2 = 0.26$) nor S1 (ANOVA: $F(1, 10) = 0.5$; $p = 0.82$; $\eta^2 = 0.005$). This supports the notion that our manipulation was indeed confined to ACC, which then triggered strong and specific downstream network effects.

DISCUSSION

Here, we demonstrate that ACC plays a central role in preventing excessively aggressive acts in a mouse model of pathological aggression—the BALB/cJ strain. We show that ACC is structurally degraded in BALB/cJ mice, exhibiting extensive neuron death coupled with a drastic loss of neuron density, an increase in the number of microglia and astroglia, as well as reactive and neurotoxic astrogliosis. Genes annotated to SNV differences between BALB/cJ and BALB/cByJ strains showed enrichment for neuronal degeneration, further confirming the notion that neuron death drives astrogliosis. Importantly, neuron loss was not a brain-wide phenomenon but focused on ACC, with limited spread to neighboring areas, such as M2. The structural degradation of ACC had functional repercussions: unlike control mice, BALB/cJ mice failed to activate ACC during aggressive encounters. Most importantly, boosting ACC activity chemogenetically prevented pathological aggressive acts, rescuing species-typical aggression. Analysis of cFos expression in downstream regions suggested that this effect may have been mediated by downregulation of “threat circuit” regions, such as BLA, LH, and VMH, and upregulation of MD, a region involved in behavioral adaptation.

One potential caveat of these results is the use of BALB/cByJ animals as a control strain. This strategy has the advantage that the BALB/cJ and BALB/cByJ strains are genetically highly similar³⁴ and differ strongly in their aggression levels, but not in potentially related traits, such as overall sociability.^{29,30,34,48} As a result, differences found between these strains are unlikely to pertain to entirely unrelated factors—one reason why previous studies have used BALB/cByJ animals as controls.^{34,49} However, BALB/cByJ animals are not identical to wild-type animals. For example, BALB/cByJ mice were found to be more anxious and less social than C57BL/6J mice.^{50,51} As such, BALB/cByJ animals are not a completely “neutral” control strain, if such a thing exists.⁵² For the current study, this would be a crucial obstacle if BALB/cByJ animals showed aberrations in aggressive behavior—e.g., by acting more tamely than a wild-type mouse. However, this seems unlikely: previous studies have reported slightly greater aggression in BALB/cByJ animals when housed in large groups,⁵³ indicating that they are not particularly tame. In this study, BALB/cByJ animals also exhibited increasing aggression on days 4 and 5 of the RI test (Figure S1A), suggesting that they develop learned aggression much like wild-type mice.⁵⁴

One of the most striking differences observed between BALB/cJ and BALB/cByJ animals was the pervasive neuron death in

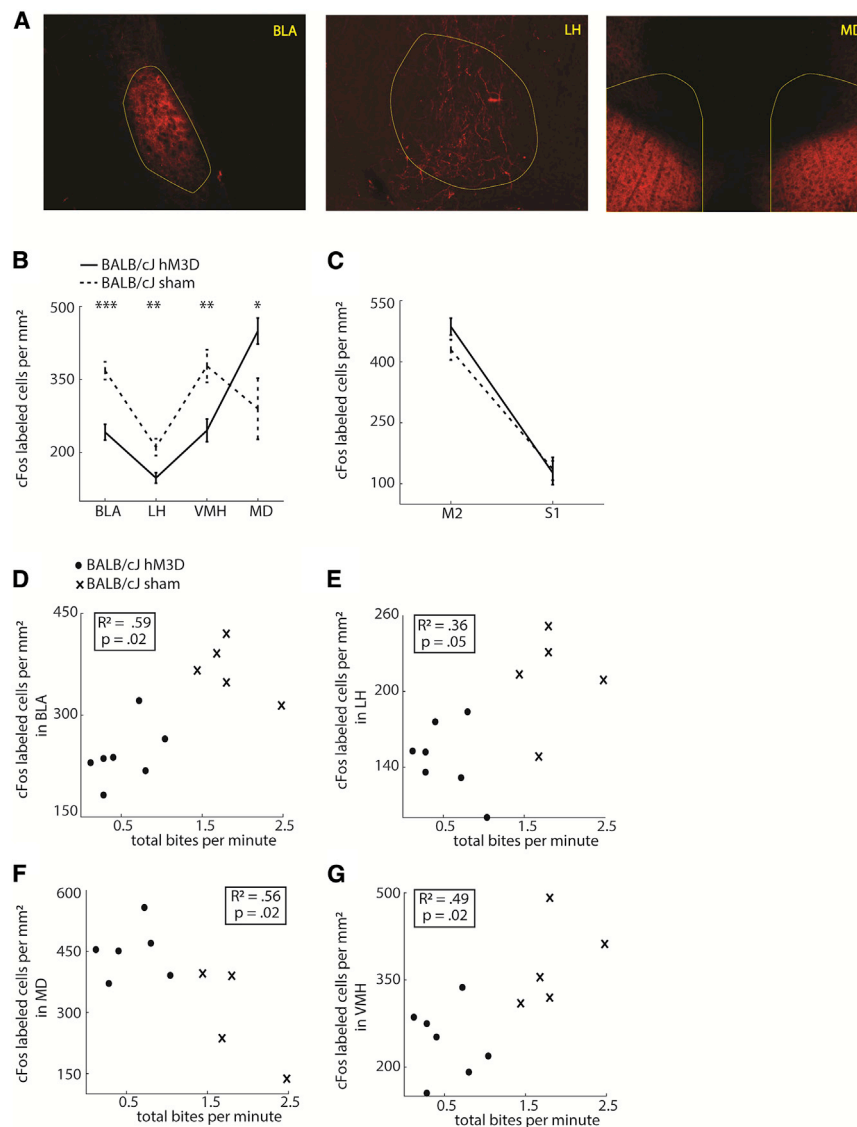


Figure 6. cFos activity in downstream regions of ACC

(A) Left: efferents of ACC in basolateral amygdala (BLA), lateral hypothalamus (LH), and mediodorsal thalamus (MD).

(B) Activity within subcortical regions. Black line, BALB/cJ mice injected with hM3D virus; dashed line, BALB/cJ mice injected with sham virus. Shown are average and SEM.

(C) Same as (B) for activity within M2 and S1.

(D) Correlation between BLA activity and average total bites per minute. Black dots, mice injected with hM3D virus; crosses, mice injected with sham virus. See in-figure legend.

(E) Same as (D) for LH.

(F) Same as (D) for MD.

(G) Same as (D) for VMH.

* $p < 0.05$; ** $p < 0.01$; *** $p < 0.001$. See also Figure S6.

point of neuronal degeneration. Loss of neuron density was largely confined to A24, leaving even directly neighboring ACC sub-regions A25 and A32, as well as M2, virtually unaffected. In contrast, neuronal degeneration was more widespread, only decreasing in more distant regions, like S1 and insula. This mismatch between widespread neuronal degeneration and localized neuron removal is consistent with a scenario in which neuronal degeneration spreads outward from ACC, followed by removal of dead neurons at a considerable delay. Such delayed removal of dead neurons has also been reported in other neuropathologies, such as Alzheimer's and Parkinson's disease.^{55–58}

If the scenario proposed here is indeed correct, it raises the question why ACC

ACC. This opens up several questions. First, does the involvement of glial populations imply that neuronal insult initiates a cascade of glial responses or that glial processes initiate neuron death? Our data indicate that neuronal insult comes first. Gene-set enrichment analysis based on SNV differences between the two BALB strains did not point to glia but highlighted several genes connected to neuronal degeneration. In addition, in neighboring M2, we observed neuron death but no indications for up-regulated toxic A1 astroglia (Figure S2), further supporting the notion that neuron death precedes glial involvement. This suggests that neuron death in ACC starts due to neuronal insult (e.g., based on developmental factors). The presence of degenerating neurons will then recruit glial processes,⁴¹ triggering reactive astrogliosis, which in turn accelerates neuron death. Crucially, is neuron death specific to ACC or does it reflect a brain-wide process? Although this question can only be answered conclusively by whole-brain analyses of neuronal degeneration, our data suggest that, at least for the young BALB/cJ animals (10 to 11 weeks) studied here, ACC is the focal

would be the “epicenter” of cell death. The key may lie in a shift of developmental processes: although neuron death occurs naturally across all brain areas during development, cingulate cortex is known to undergo a particularly high level of cell death.^{59,60} This means that, if the stop signal for developmentally necessary neuron death was to fail, continual pruning would have particularly devastating effects on cingulate cortex. The spread of neuron death from ACC to neighboring areas (Figure S2) can then be explained by a cascade of neuronal and glial signaling. Dying ACC neurons may induce a process referred to as secondary neuron loss: neurons connected to dying cells may die themselves due to the loss of synaptic input or output.⁶¹ What is more, slowed absorption of dead neurons may further spread neuronal degeneration to adjacent areas through inflammatory processes.^{37,38} If this is true, older BALB/cJ mice should show increasing levels of neuronal degeneration and neuron death across cortex. Studies on neuronal degeneration across the lifespan would therefore be required to test this hypothesis empirically.

Given the advanced structural degeneration observed in ACC, it was particularly interesting to see that simply increasing activity in the remaining ACC neurons was sufficient to induce a behavioral rescue: BALB/cJ mice that received the hM3D virus showed virtually identical behavior to BALB/cByJ mice. Specifically, ACC activation had a differential effect on aggressive behavior: species-atypical biting was almost entirely eradicated, species-typical bites were reduced less dramatically, and threat behavior remained constant. This suggests that boosting ACC activity removed the species-atypical aspects of aggression but left species-typical aggression largely intact. Based on their threat behavior and species-typical biting, it stands to reason that animals in the hM3D group still experienced the RI test as threatening, yet they were now able to respond in a species-typical way by refraining from excessive attacks.

These results further clarify the role of ACC in the control of aggressive behavior. It was previously shown that inhibiting ACC in wild-type mice during territorial challenges increases aggressive behavior, while exciting ACC eliminated aggression.¹⁷ This can, in principle, indicate that ACC curtails aggressive behavior in general. Here, we show that, rather than producing a blanket inhibition of aggressive behavior, ACC activity seems to selectively “edit” aggressive impulses, inhibiting mainly pathological expressions of aggression. When faced with an intruder, tail rattles or attacks to robust body parts are typically sufficient to settle territorial disputes, whereas potentially lethal bites to the abdomen or neck represent a species-atypical strategy. By activating ACC in BALB/cJ mice, it appears that we were able to re-instate the animal’s ability to assess the situation and adapt its actions accordingly.

This poses the interesting question what behavioral effects one would predict when manipulating ACC in wild-type animals—for instance, by activating ACC further. If our interpretation of ACC’s role as “editing” rather than suppressing aggression is correct, one would predict that ACC activation in wild-type animals would not abolish aggression but mainly redistribute it toward non-physical forms of aggression. Complementary to this, would inhibiting ACC directly increase pathological aggression? Based on previous work,¹⁷ this appears likely. However, it remains to be seen whether a transient deactivation of ACC would result in comparable behavior to that of BALB/cJ mice or whether the long-term degeneration of ACC has downstream effects (e.g., chronic hyperfunction of VHM) that would not be mimicked by a brief deactivation. In this case, a developmental mouse model with artificially induced neuron death in ACC might give clues whether structural degradation in ACC is causal to aggressive behavior. In line with this, another avenue for future research is the examination of ACC in other aggressive animal models in order to find structural changes linked to aggressive behavior irrespective of context.

Strikingly, the behavioral rescue reported here required neither a specific temporal nor spatial pattern of ACC activation but rather a simple augmentation of activity all across ACC. This suggests that a sufficient portion of different ACC subpopulations and connectivity was still present to seamlessly restore ACC’s regulatory role. This is in line with evidence suggesting that cell death does not selectively affect specific neuronal populations. Although we did not label individual neuron types in this study, we have previously demonstrated that the density of PV and

SOM interneurons decreases across cingulate cortex in BALB/cJ mice.³⁰ Given that interneurons only represent about 10% of the neuronal population, the fact that here we observed extensive neuron degeneration across all ACC layers (Figure 2B) suggests that interneurons and principal neurons are all degenerating.

Although remarkable, the fact that “blanket activation” of ACC could induce quite an intricate shift in the balance of species-typical and pathological aggression is not entirely unexpected, because previous studies using “bulk” activation of relevant cortical areas have successfully triggered complex behaviors, such as facial expressions corresponding to a specific emotion,⁶² pup approach and retrieval,⁶³ or elimination of obsessive-compulsive behaviors.⁶⁴ Our results open the door to further investigations pinpointing the circuit elements most central to the overall ACC function highlighted here. For instance, are specific neuronal subpopulations particularly instrumental to the re-instatement of ACC function? Similarly, is there a specific temporal profile of ACC activity associated with successful aggression control? Studies combining electrophysiology and optogenetics to target different neuronal populations and response dynamics would provide important insights into these topics.

How then does the blanket activation of ACC applied here accomplish selective editing of aggressive impulses? Our findings suggest that ACC efferents fine-tune the balance of activity in downstream regions: on the one hand, activating ACC increased activity in MD—a connection that has previously been shown to contribute to behavioral flexibility.^{45,46,65} On the other hand, restoring ACC activity led to a suppression of subcortical regions, particularly BLA, LH, and VMH. All three of these regions form important parts of the threat circuit (Figure 6). This also explains to some extent how ACC can reduce pathological aggression selectively by targeting downstream regions differentially: for instance, ACC projections to LH have previously been shown to be specifically involved in pathological aggression,¹⁸ whereas projections to mediobasal hypothalamus seem to affect the general incidence of aggressive behavior.

These interactions raise the question whether A24 plays a unique role within the aggression network. For instance, although our study focused on A24, other sub-regions of ACC—particularly A32—have previously also been shown to be capable of up- and downregulating aggression.¹⁷ In line with this, our cFos analyses demonstrated that the RI test resulted in reduced activation not only in A24 but also in A25 and A32 of BALB/cJ mice (Figure S3). However, we only detected limited structural changes in A25 and A32 of BALB/cJ mice: there was some neuronal degeneration but no change in neuron density or upregulation of neurotoxic glia (Figure S3). This would suggest that the structural degeneration of A24 is more central to the development of pathological aggression than that of A25 or A32. Nevertheless, the fact that manipulating different sub-areas of ACC can have comparable effects on aggressive behavior suggests that one hyper- or hypofunctioning node within the network governing aggression is sufficient to boost or impair the overall control of aggressive behavior. This is in line with studies in aggressive criminals showing a variety of lesion locations distributed across one functionally connected network.⁶⁶

Finally, the current study focused on ACC’s role in the regulation of aggressive behavior. This does, however, not preclude

that ACC might be at least as central to non-confrontative forms of social interaction (e.g., with a female animal or an inanimate object). It would therefore be interesting to probe how ACC operates in such situations. One hint that ACC degeneration may be particularly crucial to aggressive interactions is that, despite structural degeneration in ACC, BALB/cJ animals do not differ from BALB/cByJ animals when it comes to sociability.³⁰ What is more, aggression and sociability vary independently across animals, further arguing that ACC degeneration is not affecting both aspects concurrently.³⁰ This would suggest that ACC activity is less crucial to non-confrontative social interactions, enabling BALB/cJ animals to seek social contact despite ACC degeneration.

The results presented here have several implications for understanding the mechanisms underlying pathological aggression. First, previous work has shown that, even when one increases the drive to attack by manipulating activity within VMH,¹² context-sensitive control mechanisms are still in place, as certain contextual cues (e.g., presence of a female mouse) reduced aggression even during optogenetic stimulation. Our work seems to explain why: ACC utilizes such contextual cues to edit aggressive drives initiated, e.g., by VMH. When ACC activity fails, as in BALB/cJ mice, the drive to attack is not modulated, resulting in disproportionate and pathological attacks.

Reduced ACC activity has also been observed in human patients with pathological aggression,^{6,67} but there is little consensus on the underlying structural alterations. Several studies demonstrated reduced ACC volumes although others reported volume increases.^{26,68} Our data might resolve this discrepancy: as neuron degeneration sets in, glial populations will start to proliferate, which may drive increases in volume. However, as soon as degenerated neurons are removed, the volume may decrease due to neuron loss and the reduction of glial activity. Postmortem studies in patients with pathological aggression would be needed to investigate whether neuronal degeneration and reactive astrogliosis occurred. Our functional data also suggest ACC as a prime target for clinical interventions in pathological aggression: based on our results, it appears that increasing ACC activity, for example, via transcranial magnetic stimulation, may be able to address pathological aggression with minimal side effects, leaving context-appropriate aggression and patients' overall affect intact.

In conclusion, here, we demonstrate—to our knowledge for the first time—a direct and specific link between ACC activity and the control of pathological aggression. First, our data point to structural degradation as the underlying mechanism of altered ACC activity in pathological aggression. We then show that re-instating ACC activity all but eliminates pathological aggression, most likely by restoring the balance of subcortical circuits generating aggressive behavior.

STAR★METHODS

Detailed methods are provided in the online version of this paper and include the following:

- KEY RESOURCES TABLE
- RESOURCE AVAILABILITY
 - Lead contact

- Materials availability
- Data and code availability
- EXPERIMENTAL MODEL AND SUBJECT DETAILS
 - Animals & Housing conditions
- METHOD DETAILS
 - Structural and Functional Markers of ACC
 - Manipulating ACC activity
- QUANTIFICATION AND STATISTICAL ANALYSIS
 - Structural and Functional Markers of ACC
 - Manipulating ACC activity

SUPPLEMENTAL INFORMATION

Supplemental information can be found online at <https://doi.org/10.1016/j.cub.2021.03.062>.

ACKNOWLEDGMENTS

The authors wish to thank Jos Dederen and Shaghayegh Abghari for their help with all histological methods and the biotechnicians of the Preclinical Imaging Centre (Radboudumc) for all their help concerning animal testing. We thank Jean Laurens and Abdellatif Nemri for helpful comments on the manuscript. S.v.H. has been supported by a Donders Institute Top Talent grant. For the research leading to this article, J.K.B. and J.C.G. received funding from the European Community's Seventh Framework Programme (FP7/2007-2013) under grant agreement no. 602805 (Aggrosotype), no. 278948 (TACTICS), and no. 603016 (MATRICS). Further, C.F.B. and J.C.G. received funding from the Innovative Medicines Initiative 2 Joint Undertaking under grant agreement no. 115916 (PRISM). This Joint Undertaking receives support from the European Union's Horizon 2020 research and innovation programme and EFPIA. A.S.C.F. has been funded by ERC-StG 638589.

AUTHOR CONTRIBUTIONS

S.v.H. designed the study, collected and analyzed data, and prepared the manuscript; K.T., F.E.G., and S.v.D. collected and analyzed data; I.H.R. and G.P. analyzed genetic data and provided feedback on the manuscript; J.M. and J.F.V. analyzed genetic data; C.F.B., J.K.B., and J.C.G. provided feedback on the manuscript; B.A.V. conceptualized the study and provided supervision; M.N.H. conceptualized the study, provided supervision, and co-wrote the manuscript; and A.S.C.F. assisted in virus injection surgeries and fluorescence microscope data acquisition, conceptualized the study, provided supervision, and co-wrote the manuscript.

DECLARATION OF INTERESTS

J.K.B. was a consultant to/member of advisory board of/and/or speaker for Janssen-Cilag BV, Eli Lilly, Takeda (Shire), Medice, Roche, and Servier. J.C.G. has in the past 4 years been a consultant to Boehringer Ingelheim GmbH. Neither J.K.B. nor J.C.G. are employees of any of these companies, and neither are stock shareholders of any of these companies. The funding organizations or industrial consultancies listed have had no involvement with the conception, design, data analysis and interpretation, review, and/or any other aspects relating to this paper. The remaining authors declare no competing interests.

Received: November 13, 2020

Revised: February 17, 2021

Accepted: March 18, 2021

Published: April 14, 2021

REFERENCES

1. Flanigan, M.E., and Russo, S.J. (2019). Recent advances in the study of aggression. *Neuropsychopharmacology* 44, 241–244.

2. Tinbergen, N. (1968). On war and peace in animals and man. An ethologist's approach to the biology of aggression. *Science* **160**, 1411–1418.
3. Lorenz, K. (1963). *Das Sogenannte Böse* (Methuen Publishing).
4. Sapolsky, R.M. (2017). *Behave: The Biology of Humans at Our Best and Worst* (Penguin).
5. Wallace, C. (1921). Why do animals fight? *Int. J. Ethics* **31**, 264–278.
6. Blair, R.J. (2013). The neurobiology of psychopathic traits in youths. *Nat. Rev. Neurosci.* **14**, 786–799.
7. Pompili, E., Carlone, C., Silvestrini, C., and Nicolò, G. (2017). Focus on aggressive behaviour in mental illness. *Riv. Psichiatr.* **52**, 175–179.
8. Nelson, R.J., and Trainor, B.C. (2007). Neural mechanisms of aggression. *Nat. Rev. Neurosci.* **8**, 536–546.
9. Silva, B.A., Gross, C.T., and Gräff, J. (2016). The neural circuits of innate fear: detection, integration, action, and memorization. *Learn. Mem.* **23**, 544–555.
10. Hashikawa, Y., Hashikawa, K., Falkner, A.L., and Lin, D. (2017). Ventromedial hypothalamus and the generation of aggression. *Front. Syst. Neurosci.* **11**, 94.
11. Koolhaas, J.M. (1978). Hypothalamically induced intraspecific aggressive behaviour in the rat. *Exp. Brain Res.* **32**, 365–375.
12. Lin, D., Boyle, M.P., Dollar, P., Lee, H., Lein, E.S., Perona, P., and Anderson, D.J. (2011). Functional identification of an aggression locus in the mouse hypothalamus. *Nature* **470**, 221–226.
13. Hong, W., Kim, D.W., and Anderson, D.J. (2014). Antagonistic control of social versus repetitive self-grooming behaviors by separable amygdala neuronal subsets. *Cell* **158**, 1348–1361.
14. Unger, E.K., Burke, K.J., Jr., Yang, C.F., Bender, K.J., Fuller, P.M., and Shah, N.M. (2015). Medial amygdala aromatase neurons regulate aggression in both sexes. *Cell Rep.* **10**, 453–462.
15. Koolhaas, J.M. (2016). Aggression. In *Neuroscience in the 21st Century, Second Edition*, D.W. Pfaff and N.D. Volkow, eds. (Springer), pp. 2431–2447.
16. de Boer, S.F., Olivier, B., Veening, J., and Koolhaas, J.M. (2015). The neurobiology of offensive aggression: revealing a modular view. *Physiol. Behav.* **146**, 111–127.
17. Takahashi, A., Nagayasu, K., Nishitani, N., Kaneko, S., and Koide, T. (2014). Control of intermale aggression by medial prefrontal cortex activation in the mouse. *PLoS ONE* **9**, e94657.
18. Biro, L., Sipos, E., Bruzsik, B., Farkas, I., Zelena, D., Balazsfi, D., Toth, M., and Haller, J. (2018). Task division within the prefrontal cortex: distinct neuron populations selectively control different aspects of aggressive behavior via the hypothalamus. *J. Neurosci.* **38**, 4065–4075.
19. Haller, J., Tóth, M., Halasz, J., and De Boer, S.F. (2006). Patterns of violent aggression-induced brain c-fos expression in male mice selected for aggressiveness. *Physiol. Behav.* **88**, 173–182.
20. Halász, J., Tóth, M., Kalló, I., Liposits, Z., and Haller, J. (2006). The activation of prefrontal cortical neurons in aggression—a double labeling study. *Behav. Brain Res.* **175**, 166–175.
21. Siegel, A., Edinger, H., and Lowenthal, H. (1974). Effects of electrical stimulation of the medial aspect of the prefrontal cortex upon attack behavior in cats. *Brain Res.* **66**, 467–479.
22. Lischinsky, J.E., and Lin, D. (2020). Neural mechanisms of aggression across species. *Nat. Neurosci.* **23**, 1317–1328.
23. Raleigh, M.J., Steklis, H.D., Ervin, F.R., Kling, A.S., and McGuire, M.T. (1979). The effects of orbitofrontal lesions on the aggressive behavior of vervet monkeys (*Cercopithecus aethiops sabaeus*). *Exp. Neurol.* **66**, 158–168.
24. Machado, C.J., and Bachevalier, J. (2006). The impact of selective amygdala, orbital frontal cortex, or hippocampal formation lesions on established social relationships in rhesus monkeys (*Macaca mulatta*). *Behav. Neurosci.* **120**, 761–786.
25. Siever, L.J. (2008). Neurobiology of aggression and violence. *Am. J. Psychiatry* **165**, 429–442.
26. De Brito, S.A., Mechelli, A., Wilke, M., Laurens, K.R., Jones, A.P., Barker, G.J., Hodgins, S., and Viding, E. (2009). Size matters: increased grey matter in boys with conduct problems and callous-unemotional traits. *Brain* **132**, 843–852.
27. Alegria, A.A., Radua, J., and Rubia, K. (2016). Meta-analysis of fMRI studies of disruptive behavior disorders. *Am. J. Psychiatry* **173**, 1119–1130.
28. Barzman, D., Eliassen, J., McNamara, R., Abonia, P., Mossman, D., Durling, M., Adler, C., DelBello, M., and Lin, P.I. (2014). Correlations of inflammatory gene pathways, corticolimbic functional activities, and aggression in pediatric bipolar disorder: a preliminary study. *Psychiatry Res.* **224**, 107–111.
29. van Heukelum, S., Drost, L., Mogavero, F., Jager, A., Havenith, M.N., and Glennon, J.C. (2019). Aggression in BALB/cJ mice is differentially predicted by the volumes of anterior and midcingulate cortex. *Brain Struct. Funct.* **224**, 1009–1019.
30. van Heukelum, S., Mogavero, F., van de Wal, M.A.E., Geers, F.E., França, A.S.C., Buitelaar, J.K., Beckmann, C.F., Glennon, J.C., and Havenith, M.N. (2019). Gradient of parvalbumin- and somatostatin-expressing interneurons across cingulate cortex is differentially linked to aggression and sociability in BALB/cJ mice. *Front. Psychiatry* **10**, 809.
31. Wall, V.L., Fischer, E.K., and Bland, S.T. (2012). Isolation rearing attenuates social interaction-induced expression of immediate early gene protein products in the medial prefrontal cortex of male and female rats. *Physiol. Behav.* **107**, 440–450.
32. Blanchard, R.J., O'Donnell, V., and Blanchard, D.C. (1979). Attack and defensive behaviors in the albino mouse. *Aggress. Behav.* **5**, 341–352.
33. Newman, E.L., Terunuma, M., Wang, T.L., Hewage, N., Bicakci, M.B., Moss, S.J., DeBold, J.F., and Miczek, K.A. (2018). A role for prefrontal cortical NMDA receptors in murine alcohol-heightened aggression. *Neuropsychopharmacology* **43**, 1224–1234.
34. Velez, L., Sokoloff, G., Miczek, K.A., Palmer, A.A., and Dulawa, S.C. (2010). Differences in aggressive behavior and DNA copy number variants between BALB/cJ and BALB/cByJ substrains. *Behav. Genet.* **40**, 201–210.
35. Burgoyne, L.A. (1999). The mechanisms of pyknois: hypercondensation and death. *Exp. Cell Res.* **248**, 214–222.
36. Ehara, A., and Ueda, S. (2009). Application of Fluoro-Jade C in acute and chronic neurodegeneration models: utilities and staining differences. *Acta Histochem. Cytochem.* **42**, 171–179.
37. Damisah, E.C., Hill, R.A., Rai, A., Chen, F., Rothlin, C.V., Ghosh, S., and Grutzendler, J. (2020). Astrocytes and microglia play orchestrated roles and respect phagocytic territories during neuronal corpse removal in vivo. *Sci. Adv.* **6**, eaba3239.
38. Etcheagaray, J.I., Elguero, E.J., Tran, J.A., Sinatra, V., Feany, M.B., and McCall, K. (2016). Defective phagocytic corpse processing results in neurodegeneration and can be rescued by TORC1 activation. *J. Neurosci.* **36**, 3170–3183.
39. Li, T., Chen, X., Zhang, C., Zhang, Y., and Yao, W. (2019). An update on reactive astrocytes in chronic pain. *J. Neuroinflammation* **16**, 140.
40. Wilhelmsson, U., Bushong, E.A., Price, D.L., Smarr, B.L., Phung, V., Terada, M., Ellisman, M.H., and Pekny, M. (2006). Redefining the concept of reactive astrocytes as cells that remain within their unique domains upon reaction to injury. *Proc. Natl. Acad. Sci. USA* **103**, 17513–17518.
41. Liddelov, S.A., Guttenplan, K.A., Clarke, L.E., Bennett, F.C., Bohlen, C.J., Schirmer, L., Bennett, M.L., Münch, A.E., Chung, W.S., Peterson, T.C., et al. (2017). Neurotoxic reactive astrocytes are induced by activated microglia. *Nature* **541**, 481–487.
42. Perrin-Terrin, A.-S., Jeton, F., Pichon, A., Frugièrre, A., Richalet, J.-P., Bodineau, L., and Voituren, N. (2016). The c-FOS protein immunohistological detection: a useful tool as a marker of central pathways involved in specific physiological responses in vivo and ex vivo. *J. Vis. Exp.* 53613.

43. Jhang, J., Lee, H., Kang, M.S., Lee, H.-S., Park, H., and Han, J.-H. (2018). Anterior cingulate cortex and its input to the basolateral amygdala control innate fear response. *Nat. Commun.* *9*, 2744.
44. Terburg, D., Scheggia, D., Triana Del Rio, R., Klumpers, F., Ciobanu, A.C., Morgan, B., Montoya, E.R., Bos, P.A., Giobellina, G., van den Burg, E.H., et al. (2018). The basolateral amygdala is essential for rapid escape: a human and rodent study. *Cell* *175*, 723–735.e16.
45. Delevich, K., Tucciarone, J., Huang, Z.J., and Li, B. (2015). The mediodorsal thalamus drives feedforward inhibition in the anterior cingulate cortex via parvalbumin interneurons. *J. Neurosci.* *35*, 5743–5753.
46. Parnaudeau, S., Taylor, K., Bolkan, S.S., Ward, R.D., Balsam, P.D., and Kellendonk, C. (2015). Mediodorsal thalamus hypofunction impairs flexible goal-directed behavior. *Biol. Psychiatry* *77*, 445–453.
47. Hahn, J.D., and Swanson, L.W. (2012). Connections of the lateral hypothalamic area juxtadorsomedial region in the male rat. *J. Comp. Neurol.* *520*, 1831–1890.
48. Jager, A., Amiri, H., Bielczyk, N., van Heukelum, S., Heerschap, A., Aschrafi, A., Poelmans, G., Buitelaar, J.K., Kozicz, T., and Glennon, J.C. (2020). Cortical control of aggression: GABA signalling in the anterior cingulate cortex. *Eur. Neuropsychopharmacol.* *30*, 5–16.
49. Giles, J.M., Whitaker, J.W., Moy, S.S., and Fletcher, C.A. (2018). Effect of environmental enrichment on aggression in BALB/cJ and BALB/cByJ mice monitored by using an automated system. *J. Am. Assoc. Lab. Anim. Sci.* *57*, 236–243.
50. Moy, S.S., Nadler, J.J., Young, N.B., Perez, A., Holloway, L.P., Barbaro, R.P., Barbaro, J.R., Wilson, L.M., Threadgill, D.W., Lauder, J.M., et al. (2007). Mouse behavioral tasks relevant to autism: phenotypes of 10 inbred strains. *Behav. Brain Res.* *176*, 4–20.
51. Lepicard, E.M., Joubert, C., Hagneau, I., Perez-Diaz, F., and Chapouthier, G. (2000). Differences in anxiety-related behavior and response to diazepam in BALB/cByJ and C57BL/6J strains of mice. *Pharmacol. Biochem. Behav.* *67*, 739–748.
52. Beans, C. (2018). News feature: what happens when lab animals go wild. *Proc. Natl. Acad. Sci. USA* *115*, 3196–3199.
53. Bailoo, J.D., Murphy, E., Varholick, J.A., Novak, J., Palme, R., and Würbel, H. (2018). Evaluation of the effects of space allowance on measures of animal welfare in laboratory mice. *Sci. Rep.* *8*, 713.
54. Koolhaas, J.M., Coppens, C.M., de Boer, S.F., Buwalda, B., Meerlo, P., and Timmermans, P.J. (2013). The resident-intruder paradigm: a standardized test for aggression, violence and social stress. *J. Vis. Exp.* e4367.
55. Jiang, T., Yu, J.T., Zhu, X.C., and Tan, L. (2013). TREM2 in Alzheimer's disease. *Mol. Neurobiol.* *48*, 180–185.
56. Neumann, H., Kotter, M.R., and Franklin, R.J. (2009). Debris clearance by microglia: an essential link between degeneration and regeneration. *Brain* *132*, 288–295.
57. Herzog, C., Pons Garcia, L., Keatinge, M., Greenald, D., Moritz, C., Peri, F., and Herrgen, L. (2019). Rapid clearance of cellular debris by microglia limits secondary neuronal cell death after brain injury *in vivo*. *Development* *146*, dev174698.
58. Tremblay, M.E., Cookson, M.R., and Civiero, L. (2019). Glial phagocytic clearance in Parkinson's disease. *Mol. Neurodegener.* *14*, 16.
59. Fang, W.Q., and Yuste, R. (2017). Overproduction of neurons is correlated with enhanced cortical ensembles and increased perceptual discrimination. *Cell Rep.* *21*, 381–392.
60. Stankovski, L., Alvarez, C., Ouimet, T., Vitalis, T., El-Hachimi, K.H., Price, D., Deneris, E., Gaspar, P., and Cases, O. (2007). Developmental cell death is enhanced in the cerebral cortex of mice lacking the brain vesicular monoamine transporter. *J. Neurosci.* *27*, 1315–1324.
61. Fricker, M., Tolkovsky, A.M., Borutaite, V., Coleman, M., and Brown, G.C. (2018). Neuronal cell death. *Physiol. Rev.* *98*, 813–880.
62. Dolensek, N., Gehrlach, D.A., Klein, A.S., and Gogolla, N. (2020). Facial expressions of emotion states and their neuronal correlates in mice. *Science* *368*, 89–94.
63. Fang, Y.Y., Yamaguchi, T., Song, S.C., Tritsch, N.X., and Lin, D. (2018). A hypothalamic midbrain pathway essential for driving maternal behaviors. *Neuron* *98*, 192–207.e10.
64. Burguière, E., Monteiro, P., Feng, G., and Graybiel, A.M. (2013). Optogenetic stimulation of lateral orbitofronto-striatal pathway suppresses compulsive behaviors. *Science* *340*, 1243–1246.
65. Marton, T.F., Seifkar, H., Luongo, F.J., Lee, A.T., and Sohal, V.S. (2018). Roles of prefrontal cortex and mediodorsal thalamus in task engagement and behavioral flexibility. *J. Neurosci.* *38*, 2569–2578.
66. Darby, R.R., Horn, A., Cushman, F., and Fox, M.D. (2018). Lesion network localization of criminal behavior. *Proc. Natl. Acad. Sci. USA* *115*, 601–606.
67. Marsh, A.A., Finger, E.C., Fowler, K.A., Adalio, C.J., Jurkowitz, I.T.N., Schechter, J.C., Pine, D.S., Decety, J., and Blair, R.J.R. (2013). Empathic responsiveness in amygdala and anterior cingulate cortex in youths with psychopathic traits. *J. Child Psychol. Psychiatry* *54*, 900–910.
68. Boes, A.D., Tranel, D., Anderson, S.W., and Nopoulos, P. (2008). Right anterior cingulate: a neuroanatomical correlate of aggression and defiance in boys. *Behav. Neurosci.* *122*, 677–684.
69. Paxinos, G., and Franklin, K.B.J. (2013). *Paxinos and Franklin's The Mouse Brain in Stereotaxic Coordinates, Fourth Edition* (Academic).
70. Benjamini, Y., and Hochberg, Y. (1995). Controlling the false discovery rate: a practical and powerful approach to multiple testing. *J. R. Statist. Soc. B* *57*, 289–300.
71. Poelmans, G., Pauls, D.L., Buitelaar, J.K., and Franke, B. (2011). Integrated genome-wide association study findings: identification of a neurodevelopmental network for attention deficit hyperactivity disorder. *Am. J. Psychiatry* *168*, 365–377.

STAR★METHODS

KEY RESOURCES TABLE

| REAGENT or RESOURCE | SOURCE | IDENTIFIER |
|---|----------------------------|---|
| Antibodies | | |
| Iba1 anti-rabbit | Wako | product code: 019-19741; RRID: AB_839504 |
| GFAP anti-guinea pig | Synaptic Systems | product code: 173004; RRID: AB_10641162 |
| NeuN anti-chicken | Millipore | product code: ABN91; RRID: AB_11205760 |
| S100B anti-guinea pig | Synaptic Systems | product code: 287004; RRID: AB_2620025 |
| Serping1 anti-mouse | Santa Cruz | product code: sc-377062 |
| cFos anti-guinea pig | Synaptic Systems | product code: 226004; RRID: AB_2619946 |
| Alexa Fluor donkey anti-rabbit 488 | Abcam | product code: ab150061; RRID: AB_2571722 |
| Alexa Fluor donkey anti-guinea pig 647 | Jackson Immuno Research | product code: 706-605-148; RRID: AB_2340476 |
| Alexa Fluor goat anti-chicken 555 | Thermo Fisher | product code: A-21437; RRID: AB_2535858 |
| Alexa Fluor goat anti-mouse 555 | Abcam | product code: ab150114; RRID: AB_2687594 |
| Bacterial and virus strains | | |
| pAAV-CaMKIIa-hM3D(Gq)-mCherry | Addgene | catalog number: 50476-AAV5 |
| Biological samples | | |
| Brain tissue from BALB mice (see experimental models) | The Jackson Laboratory | N/A |
| Chemicals, peptides, and recombinant proteins | | |
| Clozapine-n-oxide | Enzo Life Sciences | BML-NS105-0005 |
| Critical commercial assays | | |
| Fluoro-Jade C Ready-to-Dilute Staining Kit for identifying Degenerating Neurons | VWR | BSEINTR-100-FJ |
| Deposited data | | |
| Raw data | This paper | https://doi.org/10.34973/jg6t-wp66 |
| Experimental models: Organisms/strains | | |
| Mouse: BALB/cJ | The Jackson Laboratory | Stock Number #000651 |
| Mouse: BALB/cByJ | The Jackson Laboratory | Stock Number #001026 |
| Mouse: C57BL/6J | Charles River Laboratories | Strain Code 632 |
| Software and algorithms | | |
| The Observer XT | Noldus | https://www.noldus.com/observer-xt |
| NeuroLucida | MBF Bioscience | https://www.mbfbioscience.com/neuroLucida |
| Stereo Investigator | MBF Bioscience | https://www.mbfbioscience.com/stereo-investigator |
| ImageJ | Open source | https://imagej.nih.gov/ij/download.html |
| SPSS23 | IBM | https://www.ibm.com/support/pages/downloading-ibm-spss-statistics-23 |
| MATLAB R2017b | MathWorks | https://www.mathworks.com/products/new_products/previous_release_overview.html |
| Ingenuity Pathway Analysis | QIAGEN | https://digitalinsights.qiagen.com/products-overview/discovery-insights-portfolio/analysis-and-visualization/qiagen-ipa/ |

RESOURCE AVAILABILITY

Lead contact

Further information and requests for resources should be directed to and will be fulfilled by the Lead Contact, Sabrina van Heukelum (Sabrina.vanHeukelum@radboudumc.nl).

Materials availability

This study did not generate new unique reagents.

Data and code availability

All primary datasets (unprocessed RI test videos and fluorescence images of immuno-stained brain slices) supporting the current study are publicly available here: <https://doi.org/10.34973/jg6t-wp66>

EXPERIMENTAL MODEL AND SUBJECT DETAILS

Animals & Housing conditions

For all experiments, BALB/cJ and BALB/cByJ mice were obtained from Jackson Laboratory (Bar Harbor, ME, USA) and C57BL/6J intruder mice were obtained from Charles River Laboratories (Erkrath, Germany). All mice were housed in an enriched environment (High Makrolon cages with Enviro Dri bedding material and Mouse Igloo) and had free access to dry food and water. They were kept at a reversed 12–12 h day–night cycle with sunrise at 7.30 pm. In line with the typical resident intruder (RI) protocol, test mice were housed individually, while intruder mice were housed in groups of 5–6 animals per cage. At the start of the RI test, all resident BALB/cJ and BALB/cByJ mice were 11 weeks old and all intruder C57BL/6J mice were 7 weeks old. All animal procedures were conducted in compliance with EU and national regulations as well as local animal use ethical committees (European Directive 2010/63/ EU), and approved by the Ethics Committee on Animal Experimentation of Radboud University (RU-DEC number 2013-235 & RU-DEC number 2017-0032). In total, across all experiments we tested 30 BALB/cJ mice and 13 BALB/cByJ mice in the RI test and used an additional 6 mice per strain that were not subjected to the RI test (see [Method details](#) for how many mice were used in which experiment).

METHOD DETAILS

Structural and Functional Markers of ACC

RI test

Resident mice were housed individually 10 days prior to testing. For the experiments on structural and functional markers of ACC, we tested 14 BALB/cJ mice and 13 BALB/cByJ mice across 3 different cohorts to account for possible litter effects. Aggression testing was done in the home cage of the BALB/cJ and BALB/cByJ mice in a dark room with red overhead lighting. Behavior was videotaped using an infrared camera (SuperLoLux, JVC). Animals were tested for five consecutive days, and each day each BALB/cJ and BALB/cByJ mouse was confronted in their home cage with a different C57BL/6J intruder mouse. The order of testing was randomized and the first test was started 1 hour after the beginning of the dark phase (active phase). Testing started by placing an intruder animal in the home cage of the resident animal, separated by a glass screen to allow for visual and olfactory stimulation for 5 min. After this instigation phase, the glass screen was removed and interaction was allowed for 5 minutes. In addition, we subjected 5 BALB/cJ and 5 BALB/cByJ mice (from here on referred to as cohort 3) to a slightly different protocol: we allowed interaction for 5 min *after* the first attack (up to a total maximum of 10 min). This was done to exclude the confound that BALB/cByJ mice might need longer time to show aggression as a late attack latency might influence the comparison of the total number of bites between BALB/cJ and BALB/cByJ mice. By allowing 5 min of confrontation after their first attack, all mice in this group therefore had the same amount of time to show aggressive behavior. Our results show that a prolonged confrontation phase made no difference for the BALB/cByJ mice, they were still significantly less aggressive than BALB/cJ mice also when compared to those that were tested in the shorter protocol (from here on referred to as cohort 1 & 2). After the last RI test, all BALB/cJ and BALB/cByJ mice were deeply anesthetized with isoflurane (3%–5%) and perfused with saline, followed by 150 mL of 4% paraformaldehyde solution (PFA) in 0.1M phosphate buffer (PBS). Note: mice of cohorts 1 and 2 were perfused 45 to 55 minutes after the last RI confrontation to allow for immediate early gene expression analyses. Brains were removed, fixed overnight in 4% PFA and then kept in 0.1M PBS at 4-degree temperature. 1 day before cutting, brains were placed in 0.1 M PBS plus 30% sucrose to ensure cryoprotection. Coronal sections (30 μ m) were obtained on a freezing microtome (Microm, Thermo Scientific). All sections containing ACC were placed in running order in containers filled with 0.1M PBS + 0.01% sodium azide (to prevent fungal contamination) and stored at 4-degree temperature until use.

Pyknosis, neuronal density & volumes across layers

To determine neuronal density and cell death we analyzed ACC sections of 20 BALB/cJ mice and 13 control BALB/cByJ mice. Note: of the 20 BALB/cJ mice analyzed, 6 mice did not perform the resident intruder test to control for any possible effects on density or cell death and ensure these were not the consequence of the RI test. As done in van Heukelum et al.,²⁹ we mounted sections containing A24 (ACC) on gelatine-coated slides [0.5% gelatine + 0.05% potassium chromium (III) sulfate]. Sections were then air-dried and placed in a stove at 37° overnight. The next day, sections were first placed in a 96% alcohol bath for 10 min, then hydrated in graded

alcohol baths (1 × 70%, 1 × 50%, 2 min each), dehydrated in graded alcohol baths (1 × 70%, 1 × 96%, 1 × 100%, 2 min each) and stained in a 0.1% cresyl violet solution for approximately 5 min. Afterward, sections were placed in a graded alcohol series (3 × 95%, 3 × 100%, 2 min each), cleared in xylene (Sigma–Aldrich) and mounted with entellan (Sigma–Aldrich). One image of each section was then analyzed live on an Axioskop fs microscope using Neurolucida software (MBF Bioscience). From each mouse the ACC sections were chosen at approximately the same anatomical level (ACC sections at AP 0.85). To localize A24, we used the Paxinos & Franklin mouse atlas⁶⁹ and relied on the same methodology as van Heukelum et al.²⁹ to define the start/end of each area and the border with A24. For layer measurements, we only used a subset of mice (N = 5 per strain, mice previously tested in the RI test) as these measurements required us to use all available ACC material. Next to the Cresyl-violet staining we performed a Fluoro-Jade C (FJC) staining with the FJC Ready-to-Dilute Staining Kit for identifying Degenerating Neurons from Biosensis (Catalogue number: TR-100-FJ) to identify degenerating neurons in ACC (A24), M2, S1 and insula. Sections were stained according to manufacturer's protocol with a 2-minute potassium permanganate interval and a 10-minute FJC incubation.

Microglia and astroglia across layers

To assess the number of microglia and astroglia, we used ACC sections of mice from cohort 1 and 2 (N = 9 BALB/cJ & 8 BALB/cByJ) and additionally included animals (N = 6 per strain) that did not perform the RI test to exclude effects of the RI test on glial changes (total N = 15 BALB/cJ & 13 BALB/cByJ). ACC sections were stained with a standard free-floating immunofluorescence protocol with antibodies for microglial and astroglial markers (Iba1 and GFAP and S100B respectively). Briefly, sections were incubated overnight at room temperature in Iba1 anti-rabbit (1:1500, Wako, product code: 019-19741) and GFAP anti-guinea pig (1:1500, Synaptic Systems, product code: 173004) as well as a marker for neurons (NeuN anti-chicken, 1:1000, Millipore, product code: ABN91). The following day, the sections were incubated in matching secondary antibodies at room temperature (Alexa Fluor donkey anti-rabbit 488 [Abcam, product code: ab150061], Alexa Fluor donkey anti-guinea pig 647 [Jackson Immuno Research, product code: 706-605-148] and Alexa Fluor goat anti-chicken 555 [Thermo Fisher, product code: A-21437]). Photographs of the ACC sections were then taken with an Axio Imager.A2 microscope (Zeiss) at 20x magnification. Given that GFAP in gray matter is known to often preferentially stain reactive astroglia,⁴⁰ we decided to stain for another astroglia marker, S100B, in combination with a marker for reactive toxic astroglia (Serping1). This enabled us to determine the total number of astroglia regardless their activity state as well as the percentage of toxic and neuroprotective reactive astroglia. As done previously, we used a standard free-floating immunofluorescence protocol and incubated the ACC sections overnight in S100B anti-guinea pig (1:1000, Synaptic Systems, product code: 287004) together with Serping1 anti-mouse (Santa Cruz, product code: sc-377062) as a marker for neurotoxic A1 astroglia. The next day, sections were incubated with matching secondary antibodies (anti-rabbit and anti-guinea pig were the same ones as previously used as well as an Alexa Fluor goat anti-mouse 555 [Abcam, product code: ab150114]) and a DAPI stain was added. Photographs of the ACC sections were then taken with an Axio Imager.A2 microscope (Zeiss) at 20x magnification.

Whole-genome sequencing and gene-set enrichment analysis based on genetic differences between the BALB strains

Sequencing libraries were prepared from high-quality genomic DNA using the TruSeq DNA PCR-Free kit (Illumina) and ultra-deep whole genome sequencing (average 30X read-depth across the genome) was performed on a HiSeq X Ten System (Illumina). We developed an efficient data processing and quality control pipeline. Briefly, raw sequencing data underwent stringent quality control and was aligned to either the mm10 [BALB/cJ versus BALB/cByJ strain comparison]. Isaac was used to align reads and call single nucleotide variations (SNVs). We excluded SNVs that were covered by less than 20 reads, and that were not present in both animals from the same strain. SnpEff was used to annotate SNVs and explore functional effects on gene function. As further described in the Results section, SNVs differing between the two strains were annotated to a total of 1514 genes, which were subdivided into 3 different categories (intronic/exonic non-coding and synonymous variants [1422 genes], UTR [3 & 5, 90 genes], missense mutations and splicing variants [61 genes]).

Functional activation in ACC

To assess the number of active cells, we used ACC brain sections of 15 BALB/cJ and 13 BALB/cByJ mice. As previously, for both strains we included animals (N = 6 per strain) that did not perform the RI test to check for baseline activity of ACC. ACC sections were stained with a standard free-floating immunofluorescence protocol with an antibody for cFos. Briefly, sections were incubated overnight at room temperature in cFos anti-guinea pig (1:1000, Synaptic Systems, product code: 226004). The following day, the sections were incubated in a matching secondary antibody at room temperature (Alexa Fluor donkey anti-guinea pig 647) and a DAPI stain was added. Photographs of the ACC sections were then taken with an Axio Imager.A2 microscope (Zeiss) at 20x magnification.

Manipulating ACC activity

Surgery

Fifteen 8-week old BALB/cJ mice were used for this experiment. All mice underwent stereotactic surgery and received a viral injection. Briefly, mice were anaesthetized with a ketamine-dexdomitor mix and bilaterally a small craniotomy was made at the following coordinates: 1.0 AP, 0.3 ML. A viral construct was injected (with NanoFil 10 μ L syringe, World Precision Instruments) at a depth of 1.3 DV from the brain surface. 10 mice received a bilateral 0.5 μ L injection of a viral DREADD construct (pAAV-CaMKIIa-hM3D(Gq)-mCherry, Addgene, catalog number: 50476-AAV5) at an infusion rate of 150 nanoliter per minute, to enable activation of infected neurons. After infusion, to permit the slow diffusion of the viral content, the injection needle was left in place for 10 minutes. The other 5 mice were injected with a fluorescent protein to mimic inflammation and surgical procedures and used as a control group. Mice were housed individually after surgery and testing was performed 3 weeks after surgery to allow for recovery and optimal viral expression.

Behavior

Mice were tested in the RI test for 5 consecutive days (RI test). 30 minutes before the start of the test each day, all mice received an i.p. injection of clozapine-n-oxide (CNO, Enzo Life Sciences) at a dosage of 0.3 mg/kg (working solution: 0.1 mg/mL in saline). On day 5, mice were perfused 45-55 minutes after the RI test.

Viral expression

ACC sections were checked along the rostro-caudal axis to verify the extent of (endogenous) viral expression. Three mice from the chemogenetics virus group had to be excluded due to virus expression in only one hemisphere (1 animal) and expression far beyond ACC into retrosplenial cortex (2 animals).

Immunohistochemistry

We assessed the number of active cells in ACC as well as downstream subcortical structures (amygdala, LH, VMH and MD) with a marker for cFos. For procedure please see: [Functional activation in ACC](#).

QUANTIFICATION AND STATISTICAL ANALYSIS

Structural and Functional Markers of ACC

Data analysis RI test

All behavioral measures (except attack latency) are expressed as observation per minute such that the behavior can be directly compared across cohorts. Attack behavior was scored manually in terms of attack latency, attack frequency and tail rattles using the program The Observer (Noldus). An attack was defined as a bite directed at the back, tail, abdomen, flank, neck or face of an intruder.^{29,30,34} Attacks directed to the abdomen, neck or face are considered as species-atypical bites as they have the potential to really inflict harm on the intruder.^{29,30} All recordings were scored by the same researcher who was blind to the strain of the animal (BALB/cJ and BALB/cByJ mice have the same appearance).

Data analysis pyknosis, neuron density & volume across layers

Counting was done using the optical fractionator tool in the program StereoInvestigator (MBF Biosciences), as this represents an unbiased method for cell counting. Each section had the same counting frame (50x50) and grid size (100x100). Counting was done at a 60x magnification. The *estimated population using number weighted section thickness* value given by the program was used as value for neuronal density. First, the area of each layer was delineated and then the neurons in each layer counted. Cells with a distinct nucleolus with or without several heterochromatin granules and a rim of cytoplasm around the nucleus were considered neurons. Those without a distinct nucleolus were not considered neurons. In addition, we counted those neurons showing signs of cell death. These were defined as cells with an irregular, shrunken and/or crenulated shape and nuclear shrinkage as well as increased vacuolation and tissue disruption. The total number of neurons was calculated as the sum of both healthy and pyknotic neurons per mm² (dividing the value provided by Stereo Investigator for each individual layer by the surface area of that layer). To determine the proportion of healthy neurons versus pyknotic neurons, we divided the number of pyknotic neurons by the number of healthy neurons. For volume measurements, one image of each Cresyl-violet section containing A24 was obtained. Using NeuroLucida, we then constructed contours for each cortical layer of each section separately. After constructing the contours for every ACC section, the volume per section was determined according to the following formula: area in mm² × section thickness in mm = volume in mm³. Finally, A24 volume was computed by adding up the volumes of all relevant sections. Concerning the FJC staining, the area of interest was delineated in Fiji (ImageJ), positively stained cells were counted and divided by the surface area to attain the number of degenerating neurons per mm².

Data analysis glial measures

Photographs were analyzed with Fiji (ImageJ). In short, we used the NeuN stain to outline the different layers, saved these as ROIs and then applied them to the Iba1 and GFAP stains. Microglia and astroglia were then manually counted and their number divided by the surface area of the layer to attain the number of glia per mm². Similarly, for the S100B + Serping1 double staining, layers were outlined with the DAPI stain, ROIs saved and applied to the S100B, and Serping1 stains. Positively stained cells were then manually counted and Serping1 markers were overlaid with the S100B markers to count the number of double-stained cells. The number of S100B positive cells was divided by the surface area of the specific layer and the number of A1 astroglia was determined by calculating the percentage of S100B + Serping1 double-stained cells. Percentages were transformed before applying ANOVA as analysis (arcsine transformation).

Data analysis functional activation in ACC

Photographs of the sections were analyzed with Fiji (ImageJ). Layers were outlined with the DAPI stain, ROIs saved and applied to the cFos stain. Positively stained cells were then manually counted. The number of cFos positive cells was divided by the surface area of the specific layer.

Statistical analysis RI test

Aggressive behavior was analyzed with a repeated-measures ANOVA (days as within-subject factor, strain as between-subject factor). Attack latency was analyzed separately for cohort 1-2 and cohort 3 to demonstrate that a longer confrontation time did not result in increased aggression in control mice. All other behavioral measures were analyzed together for all cohorts. All statistical analyses were carried out using SPSS23-software (SPSS, Chicago, USA). The false discovery rate method⁷⁰ was used to correct for multiple comparisons for all behavioral data. The level of statistical significance was set at $p < 0.05$. Details on the N as well as precision measures can be found in the Results section and the accompanying figure legends as well as the [Method details](#) section.

Statistical analysis histology

All contours were drawn and all counting was performed by the same researcher who was blind to the group of the animal to account for possible biases. Data was analyzed with repeated-measures ANOVAs (layer as within-subject factor, strain as between subject factor) and t tests were used as post hoc tests. The false discovery rate method⁷⁰ was used to correct for multiple comparisons. The level of statistical significance was set at $p < 0.05$. Details on the N and precision measures can be found in the [Results](#) section and the accompanying figure legends as well as the [Method details](#) section. This analysis strategy was applied to all structural (pyknosis, neuronal density, volume measurements, glial measurements) and functional measurements (cFos stain).

Statistical analysis whole-genome sequencing and gene-set enrichment analysis based on genetic differences between the BALB strains

The defined sets of genes were analyzed with IPA: based on information from the published literature as well as gene expression and gene annotation databases, IPA assigns genes to different groups and categories of functionally related genes.⁷¹ Given our histological data demonstrating neuronal death in ACC, we decided to test hypothesis-driven and focus on the category 'cell death and survival'. IPA calculates p values for the enrichment of each gene category using the right-tailed Fisher's exact test. In addition, the Benjamini-Hochberg correction was used to account for multiple testing. The level of statistical significance was set at $p < 0.05$.

Manipulating ACC activity

All behavioral and histological analyses were performed as previously described in [Data analysis RI test](#). cFos expression in ACC and downstream structures was analyzed with repeated-measure ANOVAs (either with layer or structure as within-subject factor and group [DREADD or control] as between-subject factor). Pearson-correlations between behavior and ACC activity as well as downstream activity were also calculated. The false discovery rate method⁷⁰ was used to correct for multiple comparisons. The level of statistical significance was set at $p < 0.05$. Details on the N and precision measures can be found in the [Results](#) section and the accompanying figure legends as well as the [Method details](#) section.